Compartmentalization and persistence of dominant (regulatory) T cell clones indicates antigen skewing in juvenile idiopathic arthritis

Gerdien Mijnheer[1*], Nila H. Servaas[1*], Jing Yao Leong[4], Arjan Boltjes [1], Eric Spierings[1], Phyllis Chen[4], Liyun Lai[4], Alessandra Petrelli[1], Sebastiaan Vastert[1,2], Rob J. de Boer[3], Salvatore Albani[4], Aridaman Pandit[1,#], Femke van Wijk[1,#]

[1] Center for Translational Immunology, University Medical Center Utrecht, Utrecht University, Utrecht, the Netherlands

[2] Pediatric Immunology & Rheumatology, Wilhelmina Children's Hospital, University Medical Center Utrecht, Utrecht University, Utrecht, the Netherlands

[3] Theoretical Biology, Utrecht University, Utrecht, the Netherlands

[4] Translational Immunology Institute, Singhealth/Duke-NUS Academic Medical Centre, the Academia, 20 college road, Discovery tower level 8, Singapore 169856

* These authors contributed equally

# These authors jointly supervised this work

Corresponding author: Prof. dr. Femke van Wijk, Center for Translational Immunology, Wilhelmina Children's Hospital, University Medical Centre Utrecht, Lundlaan 6, 3584 EA Utrecht, The Netherlands. Tel +31 88 75 542 75. Email: f.vanwijk@umcutrecht.nl

ABSTRACT

Autoimmune inflammation is characterized by tissue infiltration and expansion of antigen-specific T cells. Although this inflammation is often limited to specific target tissues, it remains yet to be explored whether distinct affected sites are infiltrated with the same, persistent T cell clones. Here we performed CyTOF analysis and T cell receptor (TCR) sequencing to study immune cell composition and (hyper-)expansion of circulating and joint-derived Tregs and non-Tregs in Juvenile Idiopathic Arthritis (JIA). We studied different joints affected at the same time, as well as over the course of relapsing-remitting disease. We found that the composition and functional characteristics of immune infiltrates are strikingly similar between joints within one patient, and observed a strong overlap between dominant T cell clones, especially Treg, of which some could also be detected in circulation and persisted over the course of relapsing remitting disease. Moreover, these T cell clones were characterized by a high degree of sequence similarity, indicating the presence of TCR clusters responding to the same antigens. These data suggest that in localized autoimmune disease there is auto-antigen driven expansion of both Teffector and Treg clones, that are highly persistent and are (re)circulating. These dominant clones might represent interesting therapeutic targets.

INTRODUCTION

Inflammation, often localized to specific target tissues, is a hallmark of autoimmune diseases. In these diseases, multiple sites within specific tissues can be inflamed in tandem. An example of this phenomenon includes the inflammation of multiple joints in Juvenile Idiopathic Arthritis (JIA). Multiple lines of evidence implicate T cells as key players of this tissue specific autoimmune inflammation. Firstly, many autoimmune diseases are associated with the expression of specific MHC (HLA) class II alleles, which is hypothesized to lead to altered antigen presentation and enhanced CD4+ T cell activation(1). Secondly, activated CD4+ T cells often accumulate in affected tissue(2). Lastly, $CD4^{+}CD25^{+}CD127^{low}FOXP3^{+}$ regulatory T cells (Tregs), capable of suppressing immune responses and fundamental to immune homeostasis, also accumulate in the affected tissue(3,4).

Tissue resident T cells display an array of distinct trafficking and functional markers compared to circulating T cells(5–10). Novel technologies such as mass cytometry (CyTOF) allow for high resolution analysis of the cellular heterogeneity within inflamed tissues to reveal potential pathogenic T cell populations. Moreover, studies assessing the T cell receptor (TCR) repertoire have generated evidence for the presence of clonally expanded T cells in specific tissues in autoimmune diseases(11–15). These findings suggest that tissue-specific T cell responses are mounted by specific local antigens that selectively induce activation, expansion and/or migration of antigen-specific T cell clones.

Similar to conventional T cells, Tregs that leave the thymus typically express a unique TCRs. While Tregs only represent a small fraction of the total CD4+ T cell pool, the TCR repertoire of peripheral Tregs is as diverse as that of conventional CD4+ T cells(16–18). Several studies previously showed that a restricted TCR repertoire of the

Treg compartment can lead to the development of autoimmune disease(19–22). However, Tregs with a single TCR specificity can also inhibit autoimmune responses, thereby also providing some degree of protection against autoimmunity(23). In JIA, hyper-expanded Treg TCRβ clones can be found at the site of inflammation(24–26), and in refractory JIA patients hyper-expanded Tregs can even be found in circulation(27). This expansion is likely caused by a dominance of specific (auto)antigens present at target tissues. However, the exact antigen specificity and temporal and spatial dynamics of hyper-expanded effector T cells and Tregs in chronic inflammation and their relation to disease relapses remains to be established. Defining the specific CD4+ T cell subsets that are expanding in JIA patients is critical to decipher disease pathogenesis, and hyper-expanded T cells may represent novel therapeutic targets. Moreover, insight into the antigen specificity of local T cells may aid the discovery of disease-associated autoantigens.

Here, we had the unique opportunity to study autoimmune inflammation: 1) within different affected sites at one single time point (spatial dynamics), and 2) over time (temporal dynamics), to get a detailed understanding of T cell dynamics during human autoimmune inflammation. We profiled the T cell composition of inflammatory exudate as well as peripheral blood obtained from JIA patients using CyTOF. In addition, we performed TCRβ repertoire sequencing of Tregs and conventional CD4+ T cells (non-Tregs) derived from inflamed sites of JIA patients over time and space.

RESULTS

Immune architecture of cellular infiltrates is similar between anatomically distinct inflamed sites

To study the peripheral and tissue specific immune cell composition in autoimmune disease, we profiled peripheral blood mononuclear cells (PBMCs) and synovial fluid mononuclear cells (SFMCs) from JIA patients with both knees affected at the time of sampling using CyTOF (Supplementary Table 1). T-distributed stochastic neighbor embedding (t-SNE) and k-means clustering identified 22 immune cell populations in the SF/PB compartments (Figure 1A, *P*<1e-21, Supplemental Figure 1A/B). These populations could be broadly segregated into Treg ($CD25^+/FoxP3^+$), naïve ($CD45RA^+$), effector/memory ($CD45RA^-$), and non-T cell populations ($CD3^-/CD4^-/CD8^-$). Preliminary clustering of the median marker expression on T cells revealed a clear demarcation of SFMCs and PBMCs (Figure 1B), and a strong association of immune phenotypes between intra-individual paired knee SFMCs. Furthermore, density maps of immune cell populations within the t-SNE indicate strong dichotomy in the locations of SFMC and PBMC subsets (Figure 1C). Comparison of the node fingerprints between SFMC and PBMC samples (Figure 1D) revealed that SMFCs were enriched in $CD4^+CD25^+FoxP3^+$ Tregs (node 2), and $CD4^+CD45RA^-$ memory T cells (nodes 5, 9, 10), while PBMCs were enriched in $CD45RA^+$ naïve T cells (nodes 3, 6, 7, 13, 15). Next to this, a strikingly similar cellular distribution profile was observed in the left and right knee joints of each JIA individual (Figure 1C/D). The correlation matrix of the entire spectrum of node frequencies demonstrated a strong positive correlation between the SFMCs and their left and right joints, and a strong negative correlation compared with the PBMC populations (Supplemental Figure 1C). These results demonstrate that, while distinct differences in T cell signatures can be identified between peripheral blood (PB) and synovial fluid (SF) compartments, the phenotypic T cell architecture of distinct inflamed sites (left and right knees) are remarkably similar, indicating commonality in underlying disease etiology.

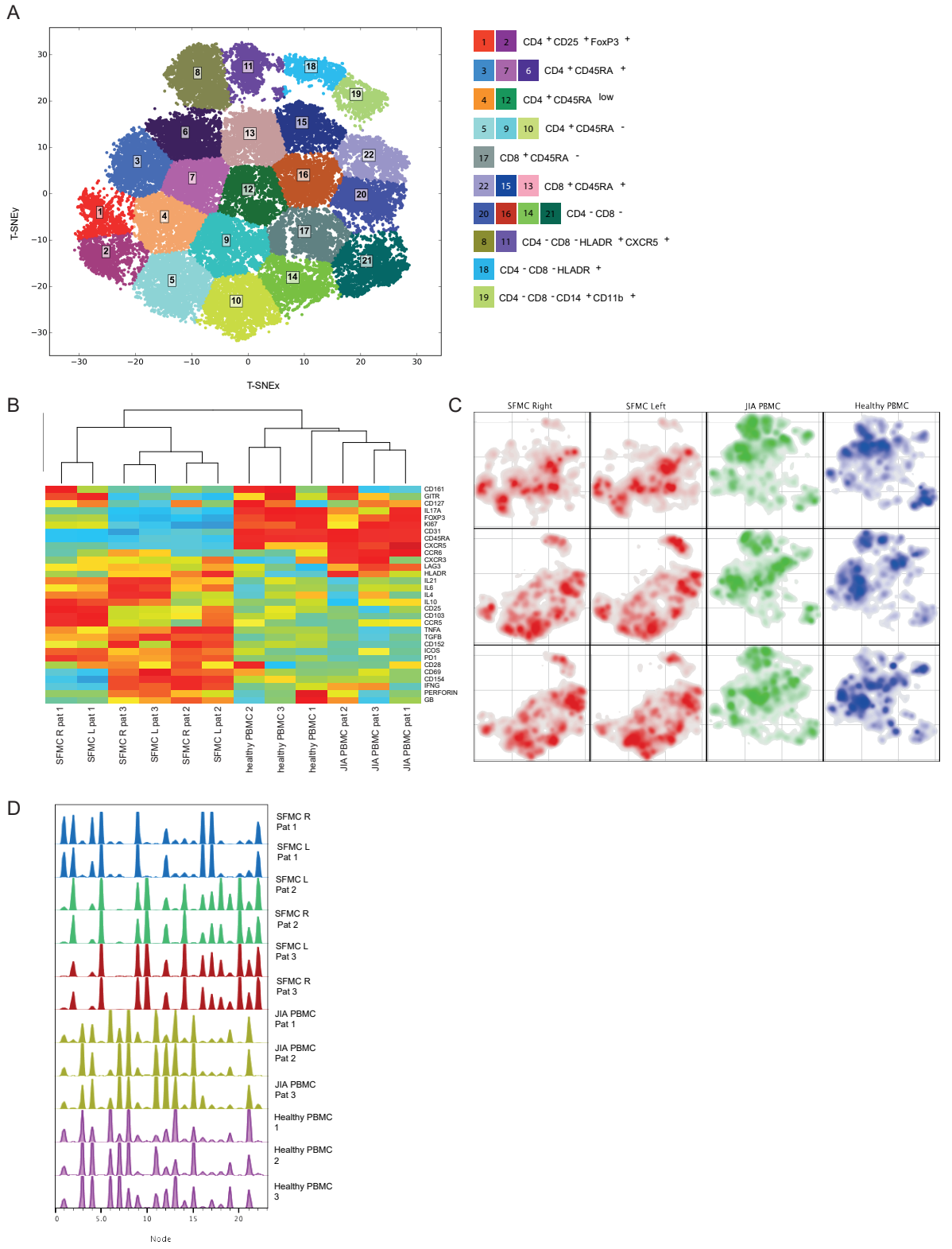

Figure 1. Overall immune architecture in left and right affected joint is very similar but distinct from peripheral blood. A. Density maps based on T-SNE dimensional reduction and k-means clustering analysis on SFMC and PBMC samples,

resulting in 22 cellular nodes. **B.** Preliminary hierarchal clustering on the median expression of all markers, excluding lineage markers. **C.** Density maps of immune cellular populations within the T-SNE maps. **D.** Node frequency fingerprints showing the distribution across the nodes of SFMCs an PBMCs.

Effector T cells and Tregs are phenotypically similar across distinct inflamed sites

Next, we functionally characterized SF specific T cells, and found that $CD4^+$ and $CD8^+$ T cell subsets displayed an increased expression of pro-inflammatory cytokines (TNFα, IFNγ and IL-6), indications of chronic TCR activation (PD1 and LAG3)(28) and a memory phenotype ($CD45RA^-$), compared to their PBMC counterparts (Supplemental Figure 2A and 2B, $P<0.05$). Remarkably, the cytokine diversity of $CD4^+$ memory T cells revealed nearly identical profiles for the left and right knee joints for each individual (Figure 2A), with minor inter-individual differences. This trend in cytokine profile was also reflected in the CD8+CD45RA- compartment (data not shown). The Treg ($CD25^+FOXP3^+$) population was significantly enriched in SF (Figure 2B, $P<0.05$, Supplemental Figure 2C/D) with enhanced expression of memory ($CD45RA^-$) and activation markers (HLA-DR/ICOS). Additionally, SF memory Tregs displayed a significantly higher proliferation (Ki67) as compared to SF effector memory T cells (Figure 2B, $P<0.05$), which was further confirmed by flow cytometry (Supplemental Figure 2E). This indicates that Tregs belong to the most proliferative T cell subset in the inflamed environment. Moreover, memory Tregs showed very similar CTLA4/HLA-DR/ICOS/PD1 expression profiles in the left and right knee joints for each individual (Figure 2C). Altogether, these data demonstrate that within JIA patients, there is an identical T cell phenotypic and functional profile present at separate

154 inflamed locations, with increased amounts of activated and proliferating Treg -
155 populations.

156

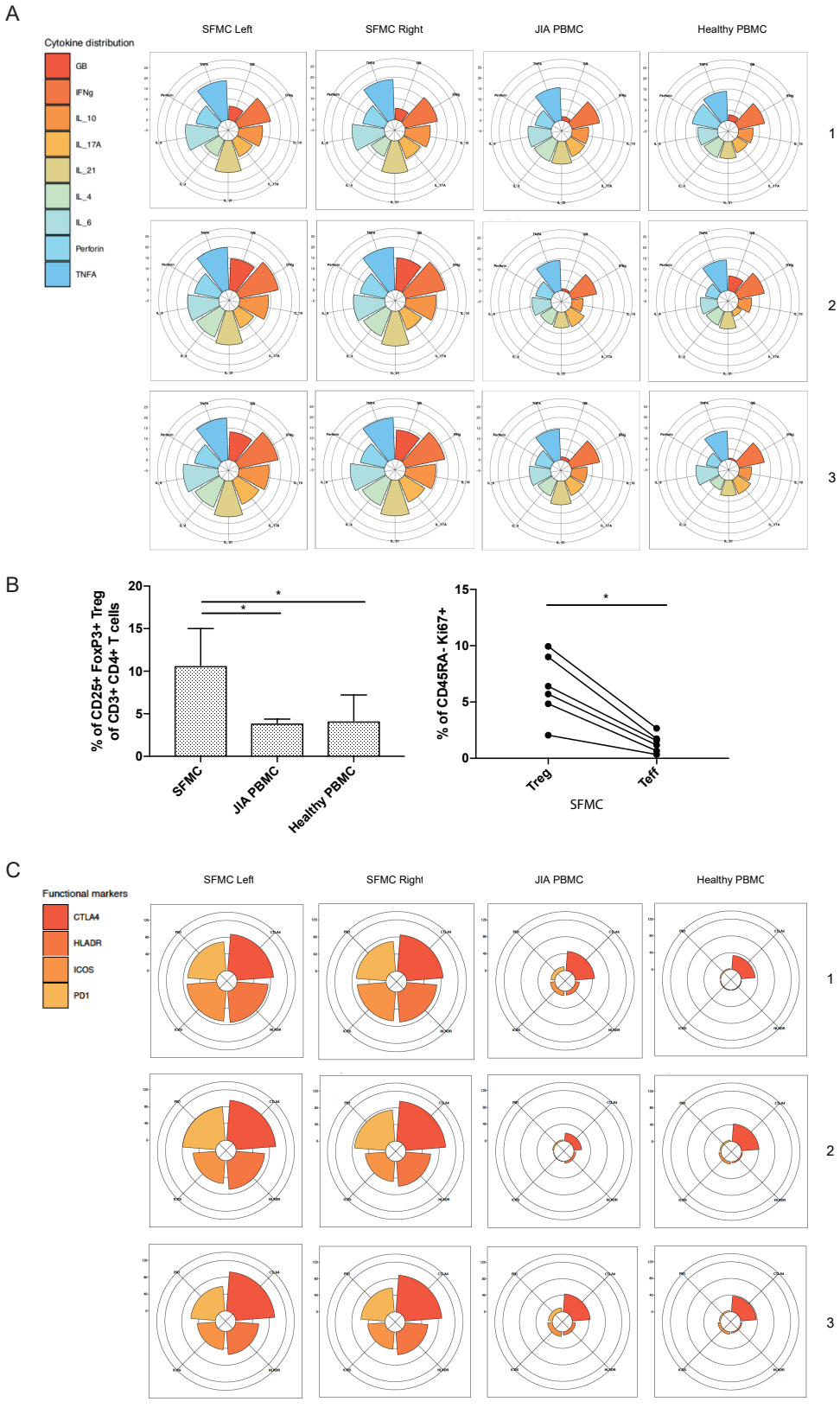

157

Figure 2. T cells display similar phenotypical and functional profiles at distinct inflamed locations. A. Cytokine production of CD4+CD45RA- memory T cells depicted in radarplots. Axis indicate the proportion of positive cells for individual cytokines (indicated by coloring) within the memory T cell fraction. SFMC = synovial fluid mononuclear cells, PBMC = peripheral blood mononuclear cells. **B.** Percentage CD25+FOXP3+ Treg of CD3+CD4+ cells in SFMC and PBMC of JIA patients and healthy children, and percentage of Ki67+ cells within CD45RA- cells in Treg and non-Treg in SFMC (non-parametric Mann-Whitney, * = $p < 0.05$). **C.** Expression of functional markers by CD25+ FOXP3+ CD45RA- cells.

Hyper-expanded T cell clones are shared between left and right joints

To study whether the same expanded T cell clones infiltrate multiple joints, we performed TCR sequencing for similar numbers of $CD3^+CD4^+CD25^+CD127^{low}$ Tregs and $CD3^+CD4^+CD25^-CD127^+$ non-Tregs sorted from affected joints of JIA patients, derived from the same donors and time points as the ones used for CyTOF analysis regarding the first two patients. Within the inflamed joints, clonally expanded cells were detected, which was more pronounced for Tregs than non-Tregs (Figure 3A). In line with the CyTOF analysis, the distribution of T cell clones was highly similar between left and right joints, both for Tregs and non-Tregs. Hyper-expanded T cells were further studied by sequential intersection of the most abundant TCRβ clonotypes across samples. We found a high degree of sharing between two affected joints, while a small fraction of clones was shared between SF and PB (Figure 3B). Moreover, sharing of clones between two joints was more evident for Tregs than non-Tregs (Figure 3B).

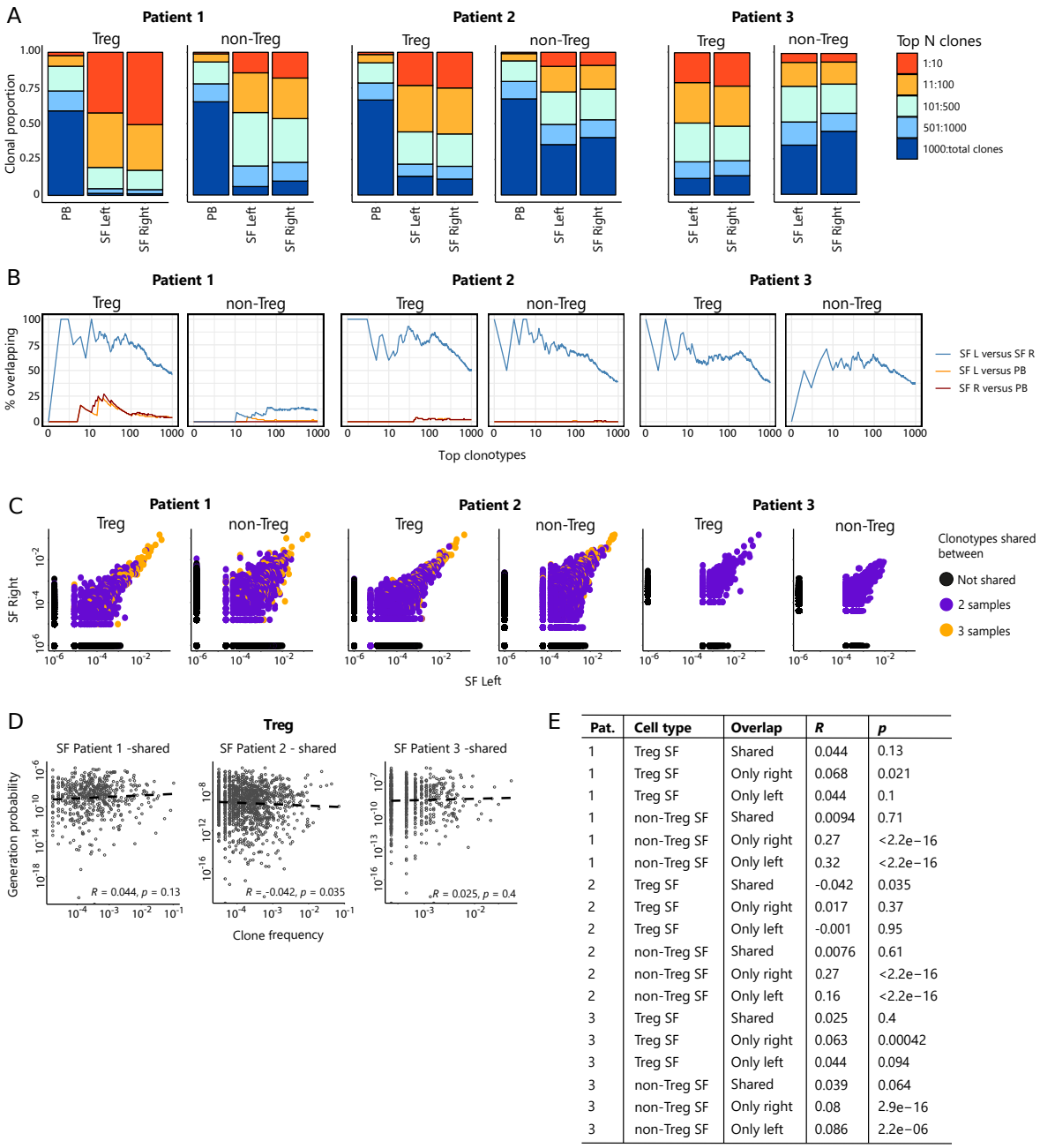

E

Pat.	Cell type	Overlap	*R*	*p*
1	Treg SF	Shared	0.044	0.13
1	Treg SF	Only right	0.068	0.021
1	Treg SF	Only left	0.044	0.1
1	non-Treg SF	Shared	0.0094	0.71
1	non-Treg SF	Only right	0.27	<2.2e−16
1	non-Treg SF	Only left	0.32	<2.2e−16
2	Treg SF	Shared	-0.042	0.035
2	Treg SF	Only right	0.017	0.37
2	Treg SF	Only left	-0.001	0.95
2	non-Treg SF	Shared	0.0076	0.61
2	non-Treg SF	Only right	0.27	<2.2e−16
2	non-Treg SF	Only left	0.16	<2.2e−16
3	Treg SF	Shared	0.025	0.4
3	Treg SF	Only right	0.063	0.00042
3	Treg SF	Only left	0.044	0.094
3	non-Treg SF	Shared	0.039	0.064
3	non-Treg SF	Only right	0.08	2.9e−16
3	non-Treg SF	Only left	0.086	2.2e−06

Figure 3. Highly dominant T cell clones are shared in SF from left and right joint and peripheral blood. A. Clonal proportions of the TCRβ clones as detected in Treg and non-Treg sorted from PBMC, SFMC left joint, SFMC right joint of two different JIA patients. **B.** Sequential intersection of abundant TCRβ clonotypes (based on amino acid sequence) across samples. Top clonotypes (ranging from 1-1000) are given on the x-axis, with the percentage of sequences overlapping between two given samples

on the y-axis. For patient 3, no PB sample was available. **C.** Frequency plots showing the overlapping Treg and non-Treg clones between left joint derived SF (x-axis) and right joint derived SF (y-axis), with color coding highlighting the clones that are shared with none of the other samples (black circle), shared in two samples (purple) and all three samples (PB, SF left, SF right; yellow). **D**. Correlation (linear regression, dashed line) between frequency (x-axis) and generation probability (y-axis) of TCR clones shared across SF two samples. **E.** Results of correlation between frequency and generation probability across all samples. Pat. = patient, *R* = Spearman's Rho, *p* = p-value, SF = synovial fluid, PB = peripheral blood.

Detailed analysis further revealed that frequencies of hyper-expanded T cells were highly conserved between distinct anatomical sites, with the most dominant clones also detectable in PB (Figure 3C). To assess whether dominant clones were shared as a result of high generation probability (P_{gen}, convergent recombination(29)), or in response to antigen (convergent selection), we calculated the P_{gens} of shared and non-shared clones and correlated these with their respective frequencies. Frequencies of shared clones were not correlated with P_{gen} (Figure 3D), while frequencies of non-shared clones showed a significant positive correlation with P_{gen} (Figure 3E). Notably, this correlation was more pronounced for non-Tregs (Figure 3E), indicating either bystander activation or non-antigen specific circulation of the non-shared TCR clones in the non-Treg compartment. In summary, both non-Treg and Treg hyper-expanded T cell clones are shared between inflamed joints. This overlap is most pronounced for Treg, with the highly dominant Treg clones in SF also being detectable in circulation, likely driven by responses to shared antigens.

Dominant clones persist over time during relapsing remitting disease

Next, to study the temporal dynamics of T cells in JIA, we profiled the Treg and non-Treg TCRβ repertoire of SF and PB samples from five JIA patients over time (Supplemental Figure 3). Repertoire overlap analysis showed that TCRβs of SF Tregs were highly shared within patients over time (Figure 4A), which was also conserved across different joints (Figure 4A/B, Supplemental Figure 4A). In contrast, TCRβs from PB did not cluster together over time, and showed much less overlap with their synovial counterparts (Figure 4A). More detailed analysis showed that frequencies of shared TCRβs were also consistent over time, with the most dominant T cell clones having the highest degree of sharing (Figure 4C). Again, this phenomenon was more pronounced in Tregs from SF compared to PB (Figure 4C), although the most dominant clones from SF were also detectable in PB (Supplemental Figure 5). Moreover, persistent TCRβs with high abundance were not driven by recombination bias (Figure 4D), similar to what was observed for T cell clones shared between two knees sampled at the same time point (Figure 3D).

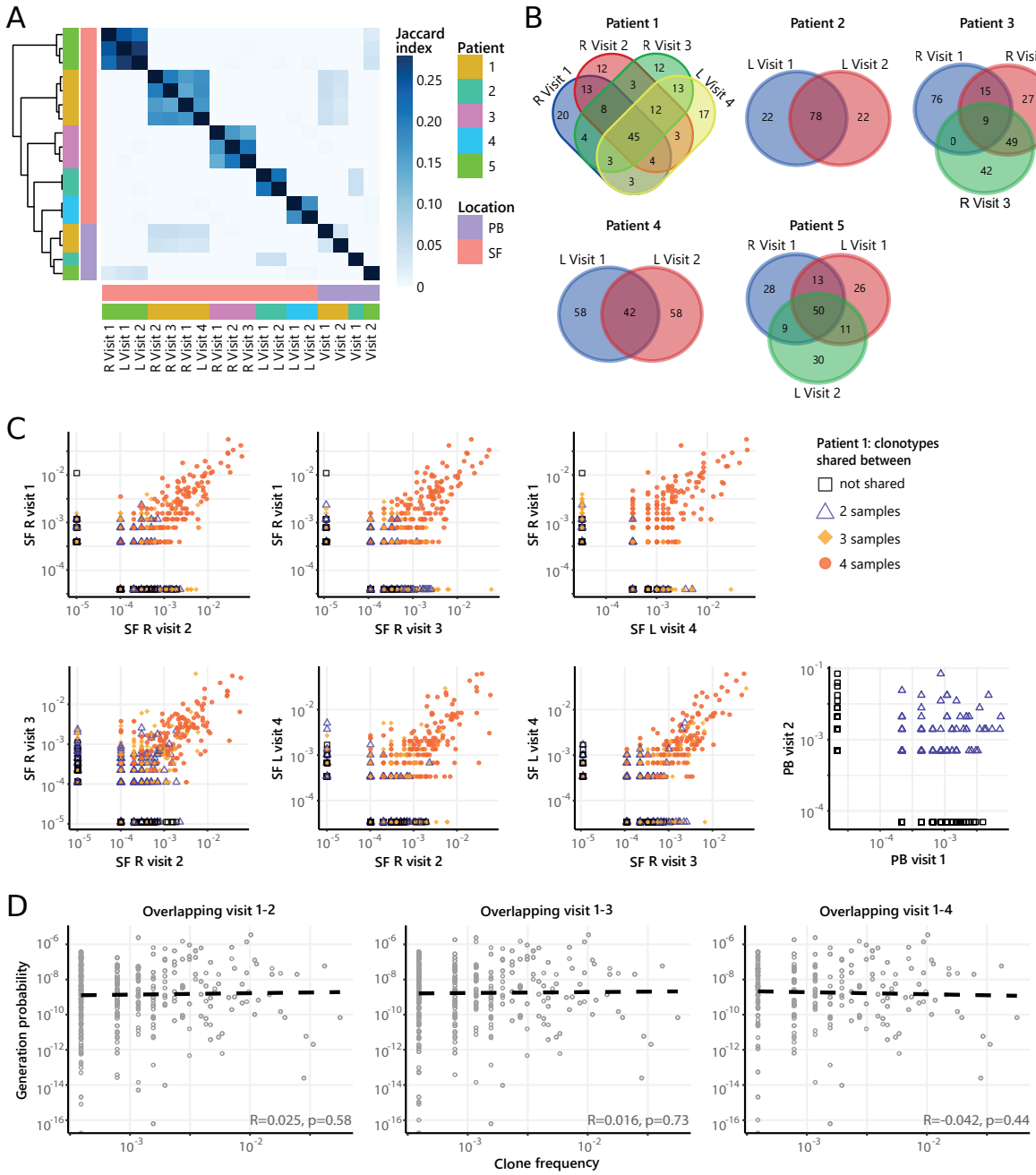

Figure 4. Persistence of Treg clones over the course of relapse remitting disease. **A.** Heatmap showing overlap (Jaccard index, light blue = limited overlap, darkblue = high overlap) of Treg derived TCR sequences obtained from SF or PB from JIA patients over time. L = left knee, R = right knee. **B.** Venn diagrams displaying the 100 most abundant unique TCRβ clones, defined by amino acid sequence, for longitudinal SF samples from all patients. **C.** Frequency plots showing the overlapping Treg clones between visits for SF and PB, with color coding and shapes highlighting the number of

samples in which unique clones are found. R = right, L = left. **D.** Correlation (linear regression, dashed line) between frequency (x-axis) and generation probability (y-axis) of TCR clones shared across two visits for SF samples.

Next, we repeated our analysis on TCRβ sequences of non-Tregs from the same samples. Although non-Tregs also display sharing of TCRβ sequences over time (Figure 5A/B, Supplemental Figure 4B), the degree of sharing was less pronounced compared to Tregs (Figure 4A). Frequencies of highly shared TCRβs in non-Tregs were also consistent over time (Figure 5C), and not driven by recombination bias (Figure 5D). Collectively, these data show that during relapsing-remitting disease, persistent dominant T cell clones are taking part in the local immune response in JIA patients, and this phenomenon is more pronounced for Tregs than non-Tregs.

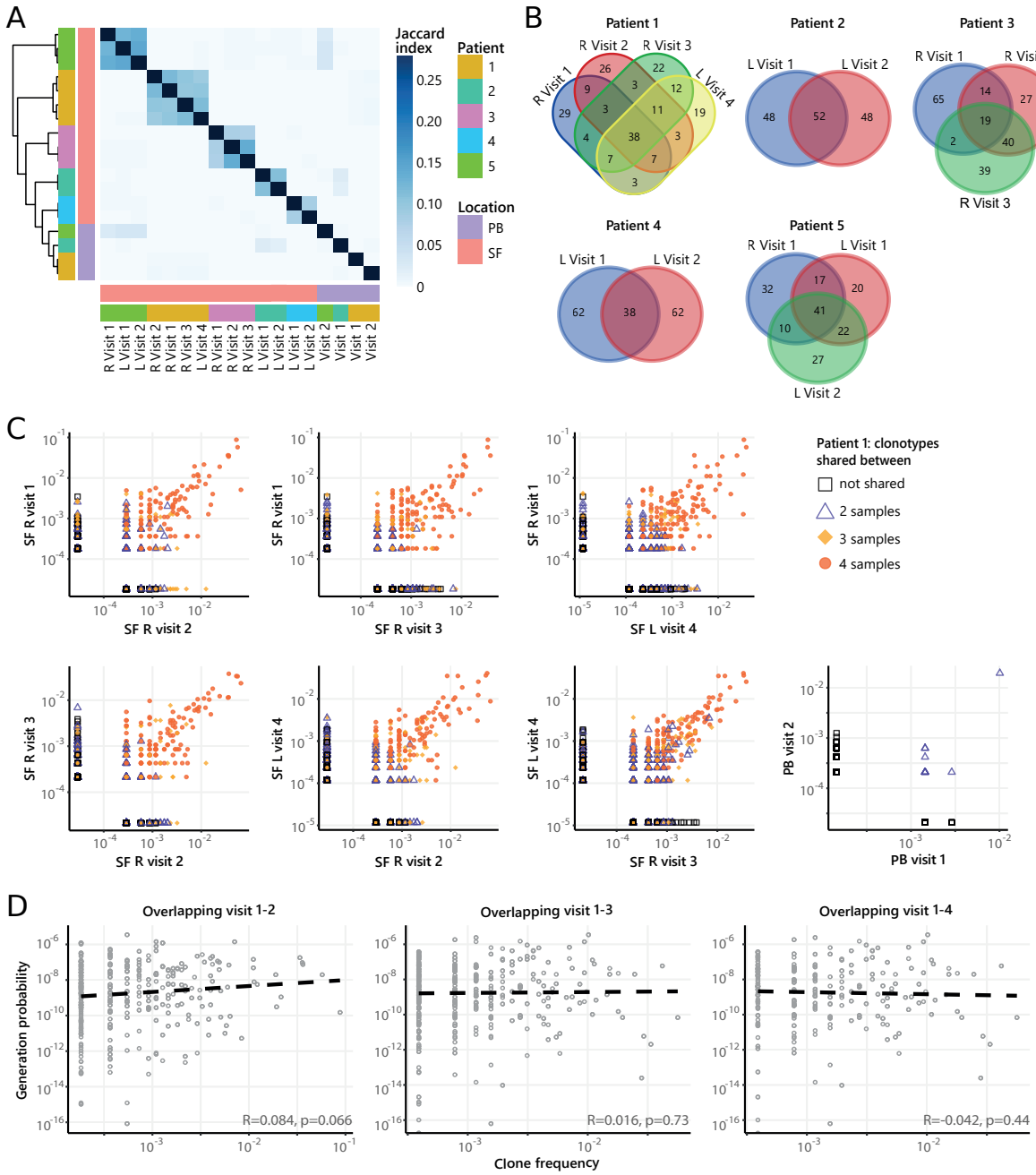

Figure 5. Persistence of non-Treg clones over the course of relapse remitting disease. A. Heatmap showing overlap (Jaccard index, light blue = limited overlap, darkblue = high overlap) of non-Treg derived TCR sequences obtained from SF or PB from JIA patients over time. L = left knee, R = right knee. **B.** Venn diagrams displaying the 100 most abundant unique TCRβ clones, defined by amino acid sequence, for longitudinal SF samples from all patients. **C.** Frequency plots showing the overlapping non-Treg clones between visits for SF and PB, with color coding and shapes

highlighting the number of samples in which unique clones are found. R = right, L = left. **D.** Correlation (linear regression, dashed line) between frequency (x-axis) and generation probability (y-axis) of TCR clones shared across two visits for SF samples.

Patterns in similar TCR sequences are shared between JIA patient knees

Recent studies have demonstrated that immune responses against a particular antigen involve T cell clones with similar TCR sequences(30–32). To investigate whether persistent T cell clones in JIA cluster together with other, similar T cell clones involved in responses against the same antigens, we performed TCR similarity analysis, focusing on SF samples obtained from two affected knees. We constructed similarity networks for JIA patients and compared these to networks generated from random repertoires with the same number of TCRβ sequences (Figure 6A). TCR networks from JIA patients were highly connected (more than expected by chance), showing that patient repertoires exhibit a high degree of sequence similarity (Figure 6B). Moreover, in the random repertoires, clusters were less mixed (indicated by a high cluster purity) than JIA networks (Figure 6C), highlighting that TCRs from JIA samples display higher sequence similarity than expected by chance. Overall, these results show that the SF Treg repertoire is highly skewed by antigenic selection.

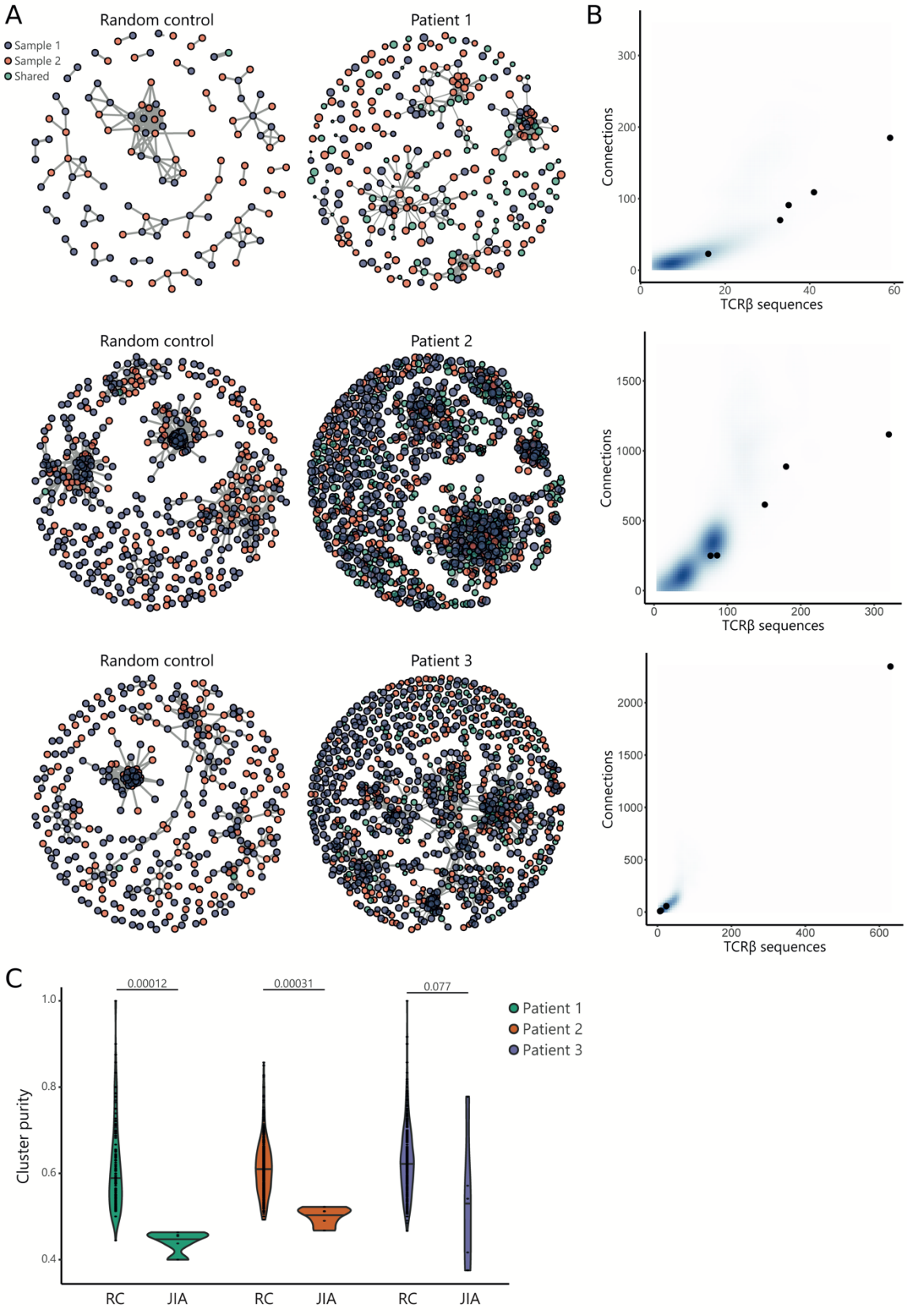

277

278 **Figure 6. TCR similarly analysis of sequences found across distinct JIA patient**

279 **knees. A.** TCR similarity networks based on amino acid k-mer sharing (k = 3) between

TCR sequences. Every node represents one TCRβ sequence, with sequences present in one sample (SF from left or right knees) highlighted in blue and orange, and sequences shared across two samples highlighted in green. Nodes are connected if TCRs share at least 8 k-mers. Networks from JIA patient repertoires (right) are compared to random repertoires (left), with the same repertoire size. **B.** Number of TCR sequences (x-axis) and their connections (y-axis) to other TCR sequences of the top five similarity clusters identified in A. Blue density maps depict clusters identified in random repertoires (N=100), while black circles depict clusters identified in JIA patients. **C.** Cluster purity (y-axis, %) for the top five clusters identified in random repertoires (RC), and JIA patient TCR similarity networks. Numbers indicate p-value of difference between RC and JIA (Mann-Whitney).

DISCUSSION

In this study, we provide the first CyTOF and TCRβ sequencing analysis of purified Tregs and non-Tregs, uncovering their spatial and temporal behavior in a human autoimmune disease setting. Although the antigen(s) driving T cell activation and expansion in JIA remain elusive, our data provide strong support for the presence of ubiquitously expressed auto-antigens given the observed overlap in dominant clones over time and in space. Given the tissue restrictive character of the JIA, it is tempting to speculate that the potential antigen would be joint-specific, although it has been shown that ubiquitously expressed auto-antigens can also induce joint-specific autoimmune disease(33,34). We show that SF Tregs have high expression of Ki67 (marking proliferation and thus recent antigen encounter), suggesting that these cells actively respond to synovial antigens. Moreover, we show that the expansion of dominant TCR clones is not dependent on generation probabilities, further highlighting

that antigen are driving T cell activation. Further support for the hypothesis that persistent, hyper-expanded Tregs found in JIA SF are auto-reactive is provided by a recent study performed in mice with type 1 diabetes, where Tregs with a high degree of self-reactivity were found to be expanding locally in affected pancreatic islets and displayed a specific profile with elevated levels of GITR, CTLA-4, ICOS and Ki67, very similar to our observations(35).

Our data demonstrated that dominant T cell clones in SF can be traced back in circulation. Together with observations that similar T cell clones are detected in multiple affected joints and the obvious overlap in immune cell composition, this strongly suggests that T cells migrate from the joint to peripheral blood and vice versa. This could mean that Tregs are either recirculating, or actively being replenished from circulating (precursor) T cells. These observations are in line with other recent studies in arthritis showing that synovial CD4+ T cells and Treg clones can also be detected in PB(25,36), where their presence correlates with disease activity and response to therapy(25,37). Moreover, for refractory JIA patients who underwent autologous hematopoietic stem cell transplantation (aHSCT), transplant outcome was shown to be dependent upon the diversity of circulating Tregs(27,37). This knowledge, combined with our findings that the same T cell clones dominate the immune response at different sites of inflammation and the persistence of the same clones in the relapsing-remitting course of disease, strengthen the possibility to use circulating disease-associated T cell clones for disease monitoring or prognostic purposes. However, to accurately monitor and predict which T cell clones from PB are implicated in active immune processes in joints, more detailed phenotyping is needed to fully characterize the functional profile and origins of dominant clones. Multi-omic single-cell profiling to link TCR specificity with gene expression will help to bring this closer to the clinic.

The existence of a temporal and spatially persistent clonal Treg TCR repertoire, raises the question to what degree clonally expanded Tregs can modulate inflammation over the course of an autoimmune response. Various studies have shown that Tregs in JIA maintain their suppressive capacity, but local effector T cells are resistant to this suppression(9,38). Thus, the clonotypic expansion in SF Treg cells might reflect an insufficient attempt to control expanding effector T cells. The importance of a diverse Treg repertoire is shown in several mouse models(19–22). Föhse *et al*. showed that Tregs with a higher diversity are able to expand more efficiently compared to Treg with a lower diversity in mice with TCR restricted conventional T cells(20). It has been suggested that this is due to the TCR diverse Tregs having access to more ligands and as a result being able to out-compete the TCR-restricted Treg cells(16). However, this applies for circulating Treg, and whether this would also be important for Treg in tissues is not known. The finding that tissue Treg residing in healthy tissues also show a considerable oligoclonality regarding their TCR repertoire may indicate that this is a normal feature(39,40). Additionally, it was recently shown that a diverse Treg repertoire in mice is especially needed to control Th1 responses, whereas Th2 and Th17 responses were still suppressed by single Treg clones(23). This could be an explanation why the Th1 rich SF environment is poorly controlled by the large amount of clonally expanded Tregs. Thus, hyper-expanded Tregs alone might not be sufficient to prevent or inhibit autoimmune responses, and future Treg centric therapies should take this into account.

In this study, we sequenced the β-chain of the TCR and not the α-chain. The identified dominant TCRβ clones can pair with several α-chains, possibly leading to less overlapping TCR repertoire and a different Ag specificity. Future sequencing of both TCR chains will provide insight into the total TCR repertoire. Next to that, we are

aware of a possible amplification bias because of a difference in efficiency of PCR primers. However, in our analysis approach we attempted to control as much as possible for such biases. An interesting next step would be to combine single cell RNA-sequencing with identification of the TCR to directly link the expression profile of a given cell to its TCR clonotype and facilitate the identification of the antigenic target and its HLA class II restriction.

In conclusion, we show that in SF the immune cell architecture is marked by inflammatory responses of activated effector T cells as well as activated and highly expanding Tregs. The remarkable overlap in immune cell composition as well as the dominant clones over time and in space provide indications for a powerful driving force that shapes the local T cell response during joint inflammation. The presence of these inflammation-associated clones in the circulation provide promising perspectives for use in disease monitoring. Moreover, the high degree of sequence similarity observed between Treg clones obtained from distinct inflamed joints indicates that antigen selection significantly reshapes the local Treg repertoire. Further research is needed to pinpoint these driving antigens and to create opportunities to target disease-specific T cells.

MATERIALS AND METHODS

Collection of SF and PB Samples

Patients with JIA were enrolled at the University Medical Center of Utrecht (The Netherlands). A total of 9 JIA patients were included in this study. Of these, n=2 were diagnosed with extended oligo JIA, n=2 with rheumatoid factor negative poly-articular JIA, and n=5 with oligo JIA, according to the revised criteria for JIA(41). The average

age at the time of inclusion was 13,1 years (range 3,2 – 18,1 years) with a disease duration of 7,3 years (range 0.4 – 14.2 years).

Peripheral blood (PB) of JIA patients was obtained via veni-puncture or intravenous drip, while synovial fluid (SF) was obtained by therapeutic joint aspiration of affected joints. Informed consent was obtained from all patients either directly or from parents/guardians when the patients were younger than 12 years of age. The study was conducted in accordance with the Institutional Review Board of the University Medical Center Utrecht (approval no. 11-499/C), in compliance with the Declaration of Helsinki. PB from n=3 healthy children (average age 15,1 years with range 14,7 - 15,4 years) was obtained from a cohort of control subjects for a case-control clinical study.

Cell isolation

For cell isolation, SF was incubated with hyaluronidase (Sigma-Aldrich, St. Louis, Missouri, United States) for 30 min at 37°C to break down hyaluronic acid. SFMCs and PBMCs were isolated using Ficoll Isopaque density gradient centrifugation (GE Healthcare Bio-Sciences AB, Uppsala Sweden), and were used after freezing in Fetal Calf Serum (FCS) (Invitrogen, Waltham, Massachusetts, United States) containing 10% DMSO (Sigma-Aldrich).

Flow cytometry and cell sorting

For TCR sequencing purposes, $CD3^{+}CD4^{+}CD25^{high}CD127^{low}$ Tregs and $CD3^{+}CD4+CD25^{low/int}CD127^{int/high}$ non-Tregs were isolated from frozen PBMC and SFMC, using the FACS Aria III (BD, Franklin Lakes, New Jersey, United States). Antibodies used for sorting were: anti human CD3-BV510 (Biolegend, San Diego,

California, United States), CD4-FITC (eBioscience, Frankfurt am Main, Germany), CD25-PE/Cy7 (BD), CD127-AF647 (Biolegend). To check for FOXP3 expression of the sorted populations anti human FOXP3-eF450 (eBioscience) was used.

CyTOF and CyTOF data analysis

Frozen PBMCs and SFMCs were thawed and stained with a T cell focused panel of 37 heavy metal-conjugated antibodies (Supplemental Table 1), as previously described(42), and analyzed by CyTOF-Helios (Fluidigm, San Francisco, California, United States). Briefly, PBMCs were stimulated with or without phorbol 12-myristate 13-acetate (150 ng/ml, Sigma-Aldrich) and ionomycin (750 ng/ml, Sigma-Aldrich) for 4 hours, and blocked with secretory inhibitors, brefeldin A (1:1000, eBioscience) and monensin (1:1000, Biolegend) for the last 2 hours. The cells were then washed and stained with cell viability dye cisplatin (200 μM, Sigma-Aldrich). Each individual sample was barcoded with a unique combination of anti-CD45 conjugated with either heavy metal 89, 115, 141 or 167, as previously described(43). Barcoded cells were washed and stained with the surface antibody cocktail for 30 min on ice, and subsequently washed and re-suspended in fixation/permeabilization buffer (permeabilization buffer, eBioscience) for 45 min on ice. Permeabilized cells were subsequently stained with an intra-cellular antibody cocktail for 45 min on ice, followed by staining with a DNA intercalator Ir-191/193 (1:2000 in 1.6% w/v paraformaldehyde, Fluidigm) overnight at 4°C or for 20 min on ice. Finally, the cells were washed and re-suspended with EQ™ Four Element Calibration beads (1:10, Fluidigm) at a concentration of $1x10^6$ cells/ml. The cell mixture was then loaded and acquired on a Helios mass cytometer (Fluidigm) calibrated with CyTOF Tunning solution (Fluidigm). The output FCS files were

randomized and normalized with the EQ™ Four Element Calibration beads (Fluidigm) against the entire run, according to the manufacturer's recommendations.

Normalized CyTOF output FCS files were de-barcoded manually into individual samples in FlowJo (v.10.2), and down-sampled to equal cell events (5000 cells) for each sample. Batch run effects were assessed using an internal biological control (PBMC aliquots from the same healthy donor for every run). Normalized cells were then clustered with MarVis(44), using Barnes Hut Stochastic Neighbor Embedding (SNE) nonlinear dimensionality reduction algorithm and k-means clustering algorithm, as previously described(42). The default clustering parameters were set at perplexity of 30, and $p<1e-21$. The cells were then mapped on a 2-dimensional t-distributed SNE scale based on the similarity score of their respective combination of markers, and categorized into nodes (k-means). To ensure that the significant nodes obtained from clustering were relevant, we performed back-gating of the clustered CSV files and supervised gating of the original FCS files with FlowJo as validation. Visualizations (density maps, node frequency fingerprint, node phenotype, radar plots) were performed through R scripts and/or Flow Jo (v.10.2). Correlation matrix and node heatmaps were generated using MarVis(44) and PRISM (v 7.0).

TCR sequencing and analysis

Tregs and non-Tregs were lysed in RLT buffer (Qiagen, Hilden, Germany) and frozen at -80°C. Between $0.15x10^6$ and $1x10^6$ Tregs, and between $0.46x10^6$ and $1x10^6$ non-Tregs were obtained for TCR sequencing. Total RNA was isolated using the RNeasy Mini Kit (Qiagen) for cell fractions $\geq 0.2x10^6$ cells and the RNeasy Micro Kit (Qiagen) for fractions $\leq 0.2x10^6$ cells, following the manufacturer's instructions. cDNA was synthesized using the SMARTer RACE cDNA Amplification kit (Clontech, Palo Alto, California, United States). Amplification of the TCRβ VDJ region was performed

using previously described primers and amplification protocols(45). PCR product fragment size was analyzed using the QIAxcel Advanced System (Qiagen). End repair and barcode adapter ligation were performed with the NGSgo®-LibrX and NGSgo®-IndX (GenDx, Utrecht, The Netherlands) according to the manufacturer's instructions. Cleanup of the samples was performed after each step using HighPrep PCR beads and following the manufacturer's instructions (GC Biotech, Waddinxveen, The Netherlands). Paired-end next-generation sequencing was performed on the Illumina MiSeq system 500 (2 x250 bp) (Illumina, San Diego, California, United States). TCR sequencing analysis was performed using RTCR as previously described(46).

TCR network analysis

For sequence similarity analysis, we counted the presence of overlapping 3-mer amino acid segments (defined as k-mers) in the TCRβ (CDR3) sequences. TCR sequences were considered similar when they shared at least 8 k-mers, independent of the total sequence length. Random repertoires were generated using the generative model of V(D)J recombination implemented in OLGA(29). For equal comparison to biological samples, random repertoires were down sampled to equal the number of TCR sequences. Cluster purity was calculated as the ratio of number of TCR sequences from the most abundant sequence within the cluster and the total number of TCR sequences in the cluster.

Statistical analyses

Nonparametric Mann Whitney (two-tailed) statistical test was performed in the manual gating of cellular subsets in FlowJo; p-values <0.05 were considered statistically significant. The correlation matrix for the node frequency was calculated

using Spearman's rank-order correlation. Generation probabilities (P_{gens}) of TCRβ amino acid sequences were computed using OLGA(29). Figures were produced using the R package ggplot2(47). Venn diagrams were made on: http://bioinformatics.psb.ugent.be/webtools/Venn/.

COMPETING INTERESTS

None declared.

FUNDING

F. van Wijk is supported by a VIDI grant from ZonMw (91714332). A.P. is supported by Netherlands Organisation for Scientific Research (NWO) (Grant number 016.Veni.178.027).

ETHICS APPROVAL

The study was approved by the board of the Local Medical Ethical Committee (METC).

DATA AVAILABILITY STATEMENT

TCR-sequencing data presented in this study have been deposited in NCBI's Gene Expression Omnibus (GEO) database under GSE196301. Both raw data and processed data are available.

REFERENCES

1. David T, Ling SF, Barton A. Genetics of immune-mediated inflammatory diseases. Clin Exp Immunol. 2018;193(1):3–12.

2. Black APB, Bhayani H, Ryder CAJ, et al. T-cell activation without proliferation in juvenile idiopathic arthritis. Arthritis Res Ther. 2002;4(3):177.

3. Wehrens EJ, Prakken BJ, van Wijk F. T cells out of control—impaired immune regulation in the inflamed joint. Nat Rev Rheumatol. 2013;9(1):34–42.

4. Long SA, Buckner JH. CD4 + FOXP3 + T Regulatory Cells in Human Autoimmunity: More Than a Numbers Game. J Immunol. 2011;187(5):2061–6.

5. Kumar BV., Ma W, Miron M, et al. Human Tissue-Resident Memory T Cells Are Defined by Core Transcriptional and Functional Signatures in Lymphoid and Mucosal Sites. Cell Rep. 2017;20(12):2921–34.

6. Nistala K, Adams S, Cambrook H, et al. Th17 plasticity in human autoimmune arthritis is driven by the inflammatory environment. Proc Natl Acad Sci. 2010;107(33):14751–6.

7. Cosmi L, Cimaz R, Maggi L, et al. Evidence of the transient nature of the Th17 phenotype of CD4+CD161+ T cells in the synovial fluid of patients with juvenile idiopathic arthritis. Arthritis Rheum. 2011;63(8):2504–15.

8. Ohl K, Nickel H, Moncrieffe H, et al. The transcription factor CREM drives an inflammatory phenotype of T cells in oligoarticular juvenile idiopathic arthritis. Pediatr Rheumatol. 2018;16(1):39.

9. Wehrens EJ, Mijnheer G, Duurland CL, et al. Functional human regulatory T cells fail to control autoimmune inflammation due to PKB/c-akt hyperactivation in effector cells. Blood. 2011;118(13):3538–48.

10. Duurland CL, Brown CC, O'Shaughnessy RFL, et al. CD161+ Tconv and CD161+ Treg Share a Transcriptional and Functional Phenotype despite Limited Overlap in TCRβ Repertoire. Front Immunol. 2017;8.

11. Muraro PA, Cassiani-Ingoni R, Chung K, et al. Clonotypic analysis of

cerebrospinal fluid T cells during disease exacerbation and remission in a patient with multiple sclerosis. J Neuroimmunol. 2006;171(1–2):177–83.

12. Chapman CG, Yamaguchi R, Tamura K, et al. Characterization of T-cell Receptor Repertoire in Inflamed Tissues of Patients with Crohn's Disease Through Deep Sequencing. Inflamm Bowel Dis. 2016;22(6):1275–85.

13. Doorenspleet ME, Westera L, Peters CP, et al. Profoundly Expanded T-cell Clones in the Inflamed and Uninflamed Intestine of Patients With Crohn's Disease. J Crohn's Colitis. 2017;11(7):831–9.

14. Günaltay S, Repsilber D, Helenius G, et al. Oligoclonal T-cell Receptor Repertoire in Colonic Biopsies of Patients with Microscopic Colitis and Ulcerative Colitis. Inflamm Bowel Dis. 2017;23(6):932–45.

15. Musters A, Klarenbeek PL, Doorenspleet ME, et al. In Rheumatoid Arthritis, Synovitis at Different Inflammatory Sites Is Dominated by Shared but Patient-Specific T Cell Clones. J Immunol. 2018;201(2):417–22.

16. Wing JB, Sakaguchi S. TCR diversity and Treg cells, sometimes more is more. Eur J Immunol. 2011;41(11):3097–100.

17. Leung MWL, Shen S, Lafaille JJ. TCR-dependent differentiation of thymic Foxp3+ cells is limited to small clonal sizes. J Exp Med. 2009;206:2121–30.

18. Wang C, Sanders CM, Yang Q, et al. High throughput sequencing reveals a complex pattern of dynamic interrelationships among human T cell subsets. Proc Natl Acad Sci. 2010;107(4):1518–23.

19. Adeegbe D, Matsutani T, Yang J, et al. CD4 + CD25 + Foxp3 + T Regulatory Cells with Limited TCR Diversity in Control of Autoimmunity. J Immunol. 2010;184(1):56–66.

20. Föhse L, Suffner J, Suhre K, et al. High TCR diversity ensures optimal function

andhomeostasis of Foxp3 + regulatory Tcells. Eur J Immunol. 2011;41(11):3101–13.

21. Yu A, Dee MJ, Adeegbe D, et al. The Lower Limit of Regulatory CD4 + Foxp3 + TCRβ Repertoire Diversity Required To Control Autoimmunity. J Immunol. 2017;198(8):3127–35.

22. Nishio J, Baba M, Atarashi K, et al. Requirement of full TCR repertoire for regulatory T cells to maintain intestinal homeostasis. Proc Natl Acad Sci. 2015;112(41):12770–5.

23. Levine AG, Hemmers S, Baptista AP, et al. Suppression of lethal autoimmunity by regulatory T cells with a single TCR specificity. J Exp Med. 2017;214(3):609–22.

24. Bending D, Giannakopoulou E, Lom H, et al. Synovial Regulatory T Cells Occupy a Discrete TCR Niche in Human Arthritis and Require Local Signals To Stabilize FOXP3 Protein Expression. J Immunol. 2015;195(12):5616–24.

25. Rossetti M, Spreafico R, Consolaro A, et al. TCR repertoire sequencing identifies synovial Treg cell clonotypes in the bloodstream during active inflammation in human arthritis. Ann Rheum Dis. 2017;76(2):435–41.

26. Henderson LA, Volpi S, Frugoni F, et al. Next-Generation Sequencing Reveals Restriction and Clonotypic Expansion of Treg Cells in Juvenile Idiopathic Arthritis. Arthritis Rheumatol. 2016;68(7):1758–68.

27. Delemarre EM, van den Broek T, Mijnheer G, et al. Autologous stem cell transplantation aids autoimmune patients by functional renewal and TCR diversification of regulatory T cells. Blood. 2016;127(1):91–101.

28. Petrelli A, Mijnheer G, Hoytema Van Konijnenburg DP, et al. PD-1+CD8+ T cells are clonally expanding effectors in human chronic inflammation. J Clin

Invest. 2018; 128(10):4669–4681.

29. Sethna Z, Elhanati Y, Callan CG, et al. OLGA: fast computation of generation probabilities of B- and T-cell receptor amino acid sequences and motifs. Bioinformatics. 2019;35(17):2974–81.

30. Dash P, Fiore-Gartland AJ, Hertz T, et al. Quantifiable predictive features define epitope-specific T cell receptor repertoires. Nature. 2017;547(7661):89–93.

31. Glanville J, Huang H, Nau A, et al. Identifying specificity groups in the T cell receptor repertoire. Nature. 2017;547(7661):94–8.

32. Pogorelyy M V., Minervina AA, Shugay M, et al. Detecting T cell receptors involved in immune responses from single repertoire snapshots. PLOS Biol. 2019;17(6):e3000314.

33. Ito Y, Hashimoto M, Hirota K, et al. Detection of T cell responses to a ubiquitous cellular protein in autoimmune disease. Science. 2014;346(6207):363–8.

34. Mandik-Nayak L, Wipke BT, Shih FF, et al. Despite ubiquitous autoantigen expression, arthritogenic autoantibody response initiates in the local lymph node. Proc Natl Acad Sci. 2002;99(22):14368–73.

35. Sprouse ML, Scavuzzo MA, Blum S, et al. High self-reactivity drives T-bet and potentiates Treg function in tissue-specific autoimmunity. JCI Insight. 2018;3(2);e97322.

36. Spreafico R, Rossetti M, van Loosdregt J, et al. A circulating reservoir of pathogenic-like CD4 + T cells shares a genetic and phenotypic signature with the inflamed synovial micro-environment. Ann Rheum Dis. 2016;75(2):459–65.

37. Lutter L, Spierings J, van Rhijn-Brouwer FCC, et al. Resetting the T Cell

Compartment in Autoimmune Diseases With Autologous Hematopoietic Stem Cell Transplantation: An Update. Front Immunol. 2018 Apr 20;9;767.

38. Haufe S, Haug M, Schepp C, et al. Impaired suppression of synovial fluid CD4+CD25− T cells from patients with juvenile idiopathic arthritis by CD4+CD25+ Treg cells. Arthritis Rheum. 2011;63(10):3153–62.

39. Burzyn D, Kuswanto W, Kolodin D, et al. A Special Population of Regulatory T Cells Potentiates Muscle Repair. Cell. 2013;155(6):1282–95.

40. Sanchez Rodriguez R, Pauli ML, Neuhaus IM, et al. Memory regulatory T cells reside in human skin. J Clin Invest. 2014;124(3):1027–36.

41. Petty RE, Southwood TR, Baum J, Bhettay E, Glass DN, Manners P, et al. Revision of the proposed classification criteria for juvenile idiopathic arthritis: Durban, 1997. In: Journal of Rheumatology. 1998.

42. Chew V, Lee YH, Pan L, et al. Immune activation underlies a sustained clinical response to Yttrium-90 radioembolisation in hepatocellular carcinoma. Gut. 2019;68(2):335–46.

43. Lai L, Ong R, Li J, et al. CD45-based barcoding approach to multiplex mass-cytometry (CyTOF). Cytom Part A. 2015;87(4):369–74.

44. Kaever A, Lingner T, Feussner K, et al. MarVis: a tool for clustering and visualization of metabolic biomarkers. BMC Bioinformatics. 2009;10(1):92.

45. Zhou D, Srivastava R, Grummel V, et al. High throughput analysis of TCR-β rearrangement and gene expression in single T cells. Lab Investig. 2006;86(3):314–21.

46. Gerritsen B, Pandit A, Andeweg AC, De Boer RJ. RTCR: A pipeline for complete and accurate recovery of T cell repertoires from high throughput sequencing data. Bioinformatics. 2016 Oct 15;32(20):3098–106.

629 47. Wickham H. ggplot2: Elegant Graphics for Data Analysis. Springer-Verlag New
630 York; 2016.

631